Results in Engineering 26 (2025) 105578

Contents lists available at ScienceDirect

Results in Engineering

journal homepage: www.sciencedirect.com/journal/results-in-engineering

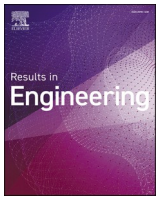

Development of CFD model for Radial Leakage Flow in a Roots Blower and Validation using Particle Image Velocimetry

Neeraj Bikramaditya, Sham Rane *, Ahmed Kovačević, Mohammad Omidyeganeh

City, St. George's University of London, London EC1V 0HB, UK

ARTICLE INFO

Keywords:
Leakage flow
Roots blower
PIV
Scorg
Radial gap
Deforming rotor grid
Smoke seeding

ABSTRACT

Oil-free positive displacement machines are used in various industries where presence of oil in the process is prohibited. Due to the lack of cooling, they experience high temperatures and thermal growth of rotors and casing. Therefore, clearances between rotors and casing are increased to avoid contact. It is important to minimise operational clearances but retain reliable operation. This requires numerical methods able to calculate leakage flows accurately. A recent PIV measurement revealed that leakage flows in radial gap of roots blower are sensitive to rotor speed. This research is aimed to perform a numerical study to evaluate various grid generation and modelling techniques for estimation of leakage flows and comparing results with data obtained by Particle Imaging Velocimetry measurements. This study considered 2D static mesh with moving wall boundary condition, 2D unsteady dynamic layering mesh and full 3D deforming rotor grid model. Additionally, to accurately replicate the shape of the rotor tip and gap size, a deforming 3D grid with filleted tip and hybrid gap model was developed. CFD model also included change in air density due to the seeding required for PIV.

Velocity magnitude and profiles in clearances, discharge flow and gas temperature predictions were validated against experimental data. Full 3D grid with hybrid gap, 5 % smoke seeding and axial gap size of 80 μm agree more with experimental data than simplified models. Discharge flow and temperature deviations from experiment were within 7 %. The validated model captured leakage flows accurately and can be applied to various rotor profile shapes.

1. Introduction

Rotary positive displacement machines find diverse applications, particularly in energy generation and conversion systems for industrial and commercial purposes. Compressed air systems account for 10 % of the total industrial energy usage and contribute significantly to the emission of greenhouse gasses. It is anticipated that they will play a pivotal role in future energy systems, particularly in compressed air energy storage [1]. Twin screw compressors take a significant share of industrial air compressors used today. Around 87 % of these compressors are oil-injected, but it is predicted that the demand of oil-free compressors will increase based on achieving clean and non-polluting gases. The development of oil-free rotary machines is having their own challenges to be addressed in terms of heat management and wear and tear of the parts [2]. This study is carried out considering a roots blower which consists of a meshing pair of straight lobes with parallel axes housed within a casing with timing gears. These types of positive displacement machines are used for low-pressure ratios of up to 2 and feature lobes generally with involute profiles. Moreover, roots blowers are oil-free positive displacement machines recognized for their simple design and moves a fixed volume of air per revolution, making them advantageous for many applications. Like other compressors, these machines also have clearance gaps namely radial, interlobe and axial. Among those gaps, the radial leakage gap accounts for major losses. The radial gap, located between the rotor tip and the casing, has been the focus of recent studies to analyse the flow field using both experimental and numerical techniques [23–25].

Clearance gaps between rotating and stationary parts in such machines is crucial for efficient and reliable operation. During the operation, thermal and pressure forces cause variations in gap sizes and influences the local flow. Kovacevic et al. [3] reported the effects of thermal distortions using fluid-solid interaction analysis. The study revealed that fluid-induced forces cause significant deformations in rotor and casing. Although deformations are small but it can have impact on performance of the machine as the clearance alters. Generally, using lower order models for the prediction of physics is less accurate, and therefore Computational Fluid Dynamics (CFD) is used for

* Corresponding author: City, St. George's University of London, London EC1V 0HB, UK.
E-mail address: sham.rane@citystgeorges.ac.uk (S. Rane).

https://doi.org/10.1016/j.rineng.2025.105578
Received 14 March 2025; Received in revised form 13 May 2025; Accepted 31 May 2025
Available online 31 May 2025

Nomenclature

P	Pressure (bar)
T_d	Torque(N-m)
N	Rotational speed (rpm)
q_{V1}	Volume Flow Rate(m^3/sec)
k	Specific heat ratio(gas)
v	Velocity (m/s)
η	Efficiency
ω	Rotational velocity(rad/*sec*)
V	Volume (m^3)

Acronyms

PR	Pressure Ratio
RPM	Rotation per minute
CFD	Computational Fluid Dynamics
PIV	Particle Image velocimetry
μm	Micrometres
MRF	Moving Reference Frame
SMM	Sliding Mesh Method
RANS	Reynolds Averaged Navier Stokes
URANS	Unsteady RANS
DNS	Direct Numerical Simulation

leakage flows study and performance prediction as outlined by Kovačević et al. in [4]. Another study by Kovačević & Rane [5] mentioned the challenges of modelling 3D CFD for rotary positive displacement machines indicating the need for good quality mesh and adequate refinement to calculate single-phase or multiphase flows. A study carried out by Kovačević et.al [6] indicated the influence of the CFD solver on the prediction of results. They reported differences in the results while comparing two different approaches namely segregated cell-center based and coupled vertex-center based schemes. The study indicated the future aspects of numerical simulation based on the use of different solvers and grids technologies by comparing results with the test. The same also on the performance of oil-free compressors with moving boundaries have outlined the transient characteristics of flow, making numerical models challenging in terms of grid generation technology, topology, and refinement.

Several papers report on how to address the issues of grid generation in screw machines. Rane et.al [7] investigated the key-frame re-meshing technique which supplies pre-generated unstructured grids to the solver at different time steps. In their study, they analyzed three strategies namely diffusion equation mesh smoothing, user-defined nodal displacement analytical method and key-frame remeshing. They concluded that existing grid deformation strategies had significant limitations for the complex geometry of screw machines. Therefore, they sought for the development of customized grid generation tools specifically for these machines. One of the significant developments in grid generation for rotary PDMs was reported by Rane & Kovačević [8] and its validation in literature [9] for a dry twin screw compressor. This work builds on the foundation of pioneered work on grid generation method by Kovačević et.al [10] for screw rotors using an algebraic method that featured boundary adaption and transfinite interpolation. The single-domain computational grid generation method is based on casing-to-rotor topology resulting in the elimination of the non-conformal interface between Rotors, which are incorporated in the SCORG a deforming rotor grid generation software based on the pioneer research work by Kovačević [11] in his thesis. Ye et al. [12] has reported in their CFD simulation of rotary vane energy device for waste heat recovery that rotational speed and tip clearance have significant effect on performance. To discretize rotating and deforming domain, they innovated analytical approach based on user defined nodal displacement. They notified that the axial clearance contributed to the 2.9 % loss of the volumetric losses. Ye et al. [13] in their another research presented a new analytical grid generation method for sliding vane rotary machine based on user defined nodal displacement approach. Their investigation reported that the developed method can be used for broader range of design configuration. The comparison between different approach available for meshing and current, new analytical grid found to be significantly faster. Neeraj et al. [14] performed initial study on modelling of radial tip gap of roots blower using moving reference frame method and simulated the effect of different combinations of the tip profile to find leakage flow amount. Most of the previous researches on CFD applications to screw machines features innovative techniques for generating meshes to adequately resolve flows in clearances. However, an alternate approach is demonstrated by Rowinski et.al [15] utilizing the automatic grid generation based on a modified cartesian cut-cell technique. This approach was used in the 3D CFD modelling of the hook and claw type hydrogen pump by Lu et al. [16]. It was reported that the simulation setup is simpler for this technique and facilitates the creation of dynamic grids which can represent the intricate and moving boundaries. Theofanidis et al. [17] performed CFD simulation using cut-cell Cartesian meshing method to handle complex moving geometry to investigate the influence of discharge port. Tutar et al. [18] presented a literature on Lattice Boltzmann method to simulate thermodynamic process of tri-rotor compressor using thermodynamic computational modelling approach. This approach eliminates the use of time-consuming classical fluid domain meshing. This study also validated their modelling with experiment results. Ma et al. [19] reported a CFD simulation using CFX of internal flow field in the dry screw vacuum pump using structured dynamic grid. They also indicated that the clearance is the most important factor affecting the performance of the vacuum pump.

Various research efforts have been reported on the investigation of leakage flow in clearance gaps experimentally and numerically. Other than grid technology, numerical models are also affected by the specification of boundary conditions and turbulence models. Kauder & Stratmann [20] reported work on using different turbulence models to predict velocities in the clearance gap numerically and its validation using the Schlieren experiment. In another study in terms of a different approach to defining physics, Vimmr & Fryc [21] analysed a 2D simplified numerical model of a screw compressor using the Moving Reference Frame and reported that the speed of the rotor has a negligible effect on the flow field inside clearance gap at a given pressure ratio. Using a more realistic method to define flow in the machine, Sun et al. [22] established a 3D Unsteady numerical model of a roots blower to study the internal flow field in the gaps. In their extended study in literature [23], Sun et al. conducted a study on Roots vacuum pumps, where they validated the flow field in the working chamber and the inlet/outlet pockets using 3D unsteady flow simulation. Further, Sun et. al [24] used a numerical model of roots blower in reference [22] to predict the flow field and its validation with PIV. They found that flow losses in the tip gap mainly happen at the entrance of the gap. Using the setup discussed in [24], Singh et al. [25] validated numerical models against PIV data in the clearance gap. This study discussed the effect of the clearance gap on the overall flow field using different rotational speeds and at different crank angles. They utilized deforming rotor grid generated in SCORG [11] with casing-to-rotor conformal topology reported by Rane et.al [7–9]. Similar research has been performed using other types of compressors. One of them is a study by Zhang et.al [26] on a scroll-type hydrogen pump using a 3D deforming grid and transient model. They reported that the deviation of CFD results by 9 % from the test.

Few other studies have been carried out using fluid-structure interactions for the analysis of leakage flow. Chen et al. [27] employed the immersed boundary method to simulate unsteady flows in a compressor, utilizing a turbulent wall model established by Tamaki et al. [28]. The method demonstrated promising results in comparison to the test data.

Other study using fluid-structure interactions by Seyyed et al. [29] have utilized the partitioned FSI approach. This method enables the separate simulations of fluid and solid mechanics in interactive way. Using a different method known as the fictitious domain method for the simulation of the compressible flow in a rotary volumetric pump was reported by Voorde et al. [30]. This study discussed the incompatibility of such methods for compressible flows because flow with variable density, enforcement of a kinematic restraint is not equivalent to enforcement of a mass flux. They noticed large back-flow through the rotors which made pressure build-up almost impossible. Considering the effect of the selection of boundary conditions, Coull & Atkins [31] studied the influence on Tip leakage flow in a gas turbine. They reported that the cascade of inlet condition and relative casing motion of the turbine rotor have a significant effect on the pattern of leakage flow. In the extension of work in [31], a study was performed by Maynard et al. [32] on the unsteady structure of compressor tip leakage flow using DNS to identify the flow structure in the tip flows. They reported that the shape of the corner of the tip are the main cause of altering flow steadiness. Many researchers have preferred SST K-omega turbulence models over many available models for rotary machines. Praveen et al. [33] utilized SST K-omega in their Fluid- Structure Interaction modelling of wind turbines to find out the lifespan of blade by introducing a small cracks and holes in main geometry. These irregularities were then analysed by loads, deflection and stress levels.

Applying various approaches discussed earlier which are based on different physics setups, grid generations and problem formulation to improve the overall numerical prediction, researchers have tried to understand the physics of fluid flow using heat transfer in the clearance by developing the conjugate heat transfer models. Patel et.al [34] used conjugate heat transfer simulation and validated the model using an Infrared Thermography test data obtained in this research. They also outlined the need for improvements towards the CHT model. A Research work by Henshaw & Chand [35] proposed a new numerical method for modelling temperature dependent fluid flow and coupling to heat transfer in solids ability to compute transient and steady state problems. They used centred discrete approximations to the interface equations. They also reported future directions related to the use of this method in deforming solid cases. One study on turbulent convective heat transfer in rotor-stator systems by Dang et al. [36] used the numerical technique of mixing plane model for coupling the rotating and stationary domains to improve the CHT. Rane et al. [37] developed a bi-directional system coupling for CHT and variable leakage gap CFD analysis of twin-screw compressors. In this study, the deformation of the rotor was calibrated to match the test results. Another study on CHT was done by Mario et al. [38] using a roots blower and its validation with the infrared thermography test results. A comprehensive study on the effect of heat transfer using conjugate heat transfer modelling on the overall flow was presented by Ding et al. [39]. They established an innovative approach to conjugate heat transfer using the Mixed Timescale Coupling method between different media. This approach can address the time scale difference in the propagation of heat in both the fluid and solids. Recently, Ding et al. [40] established a two-way coupling of CFD conjugate heat transfer with solid thermal expansion in twin screw compressors to accommodate the change in the size of the gaps from deformation. They used Simerics-MP+ solver generated mesh and Mismatched Grid Interface (MGI) to connect the fluid volumes. Wang et al. [41] used a variable pseudo density for solids in the simulation of the transient heat transfer characteristics between the compressed gas and the solid. They found that the pseudo-density method gives similar numerical accuracy as other coupled methods, and it is significantly low in computational cost. A study by Cai et al. [42] that formulates a correlation for the coupling error, together with the Proportional-Integral-Derivative (PID) control method, to propose an adaptive fluid-solid coupling time step algorithm, which dynamically adjusts the coupling time step such that the computational efficiency can be improved without sacrificing accuracy.

Meanwhile, a recent experimental study by Brijesh et al. [43] used a PIV setup to measure radial leakage flow through optical access under machine operating conditions. The optical access was created using sapphire glass assembled by removing part of casing material. The use of sapphire glass increased the radial gap from 0.1 mm to 0.72 mm because of the sealings to avoid external leakage passage. The velocity data was captured at 45° crank angle of tip and at 20 mm far from one of the axial ends. There is more description is written in methodology section. They found that the rotational speed of the rotor at a pressure ratio affects the leakage flow field and velocity field is higher at RPM1800 than RPM2000 at given pressure ratio. Also, the flow field was found to be discontinuous in the clearance gap and wake. These results obtained by Patel et al. [43] are in contradiction with past studies by Vimmr et al. [21]. Since the recent PIV test has indicated that the flow field is affected by the change in rotor speed and fluid flow changes it's gradient, it is

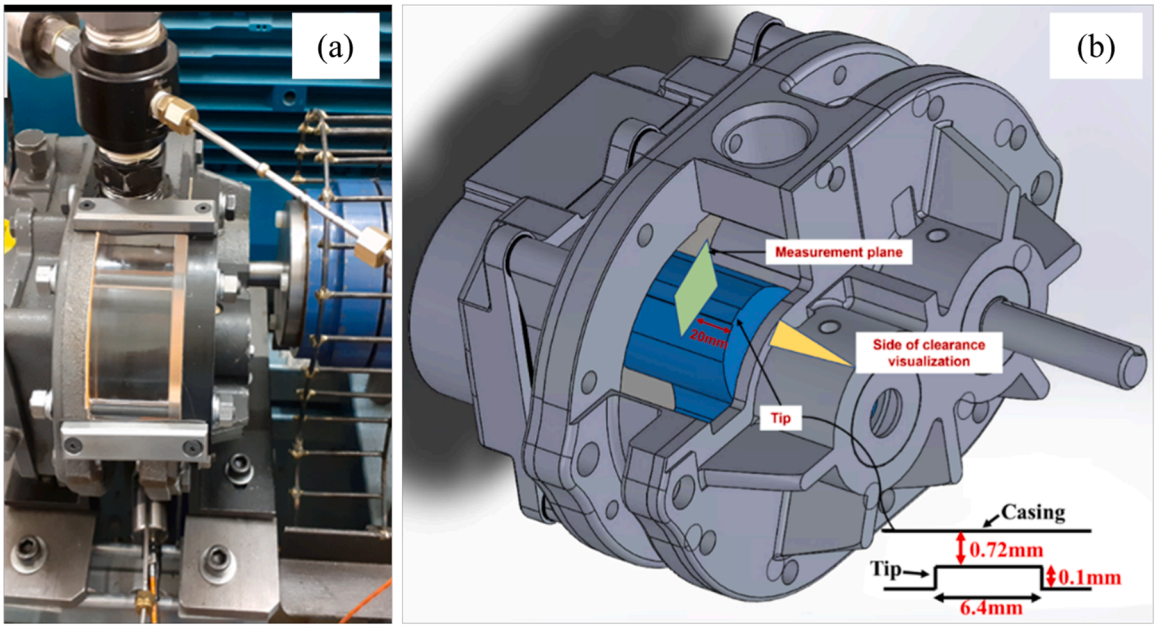

Fig. 1. (a) Radial optical access of Roots blower (b) Measurement plane, position and Tip dimensions.

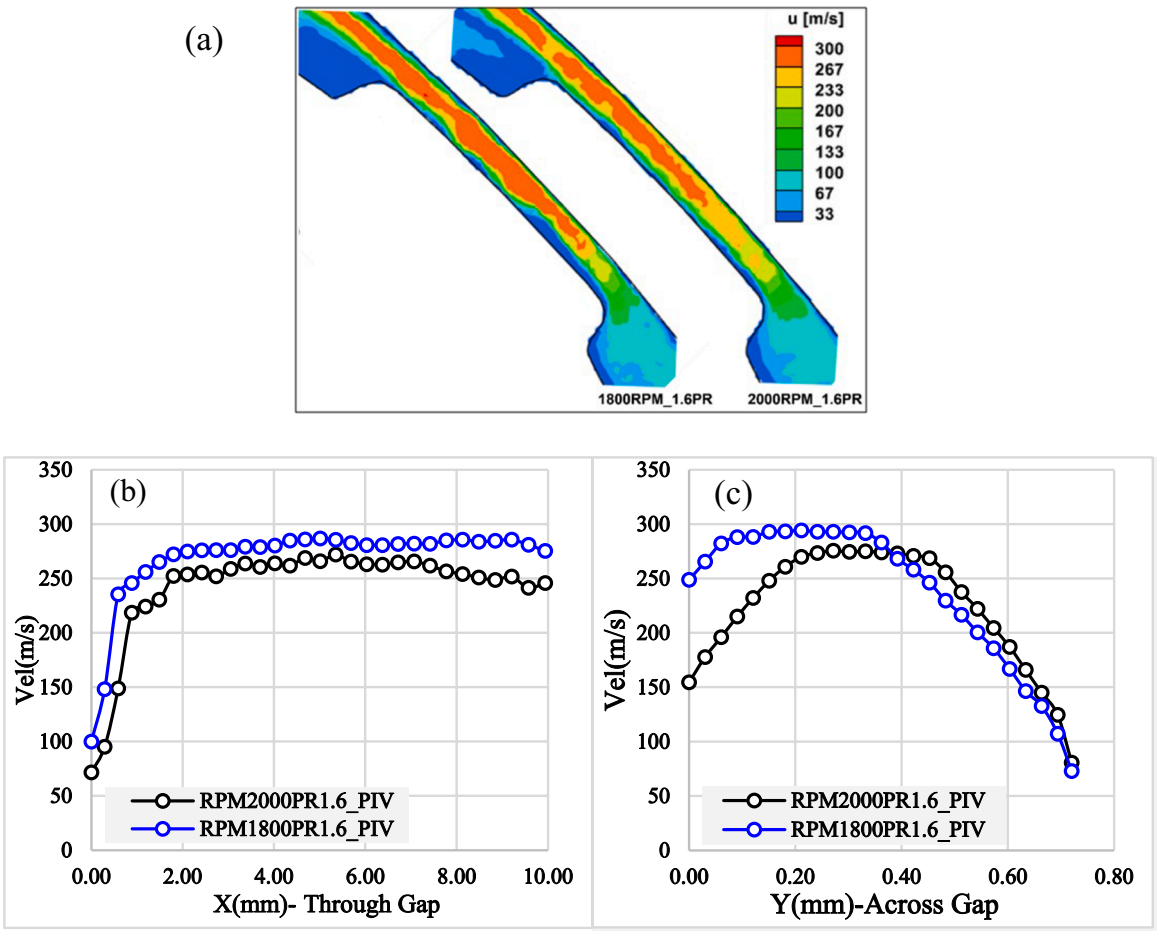

Fig. 2. (a) Velocity contour, (b) & (c) Velocity profile through & across the gap at PR1.6 respectively.

important to compare these findings numerically by improving current methodologies.

While researchers have made significant advancements in grid generation techniques, utilizing different approaches and turbulence models to enhance the accuracy of leakage flow models, conducting in-depth numerical analysis of leakage flow in radial gap and its verification with experiments is lacking. The numerical study presented here aims to investigate the radial leakage flow dynamics using variety of modelling approaches. A number of techniques starting with the simplified model to realistic 3D model are presented in order to compare and improve understanding of challenges and benefits of each method. First, modelling, analysis and comparison was made between two simplified models of a static mesh with moving wall boundary specified at the rotor tip, and an unsteady dynamic layering mesh technique for moving mesh. In the second step, the 3D deforming rotor grid was used as presented in [25]. Issues of the change in the tip profile was identified. To address the issues identified in 3D deforming rotor grid, study developed a grid which maintains the profile of the rotor and capture the tip fillet accurately. Furthermore, the test setup contained an optical access to the leakage gap for capturing velocity field using Particle Image Velocimetry (PIV). This study extended the development of grid to accommodate the assembly of the optical window. Finally, the study considered to include modelling of smoke and air mixture by altering the molecular weight of the fluid composition, to match the condition of seeding in PIV test. The same modelling technique can also be applied to different profiles of the tip and different types of smoke seeding.

2. Methodology

This section outlines the experimental test setup and various numerical simulation schemes employed to analyse the leakage flow through the radial gap of the Roots blower. In addition, the numerical schemes of steady mesh with moving wall boundary condition, unsteady dynamic layering mesh technique and finally a full 3D deforming rotor grid approach will be described in detail. This section also explains modelling of the seeding with smoke.

2.1. Particle image velocimetry set-up

An experimental study of radial leakage flows in a Roots blower using PIV measurements is detailed in [43]. The Particle Image Velocimetry (PIV) is an optical velocity measurement technique which provides quantitative measurement of instantaneous and mean velocities. In this setup, an optical access through the sapphire glass window was used for the measurement of velocities in the radial clearance gap of Roots blower. The glass window was used to replace a small section of the casing on the side of the driven rotor. Fig. 1(a) illustrates the assembly of the installed glass window. As shown in Fig. 1(a), optical access was provided from both radial and axial directions. The radial access is used to illuminate the domain with a laser sheet while the axial window is utilised for visualization of flow in the radial clearance gap between the rotor tip and the housing using a high-speed camera. Due to the setup of the glass assembly, the tip clearance gap between the lobe tip and the glass was increased from the nominal 0.1 mm to 0.72 mm, as shown in Fig. 1(b). The gap size is a significant parameter which affects flow in clearances. The suction flow is seeded by smoke to provide

Table 1
Experiment Input conditions.

PR	RPM	P_{out}/P_{in} [kPa]	T_{out}/T_{in} [K]
1.6	2000	161.2/100.8	425.0/305.0
	1800		418.0/304.0
1.2	2000	121.6/100.8	330.8/303.1
	1800		330.1/302.5
	1500		332.1/302.1

Table 2
Reference performance measurements.

Pressure Ratio	Speed [RPM]	Discharge Temp [°C]	Discharge flow rate [kg/s]	Torque [Nm]	Spec Power [kW/m³/min]
1.203	1500	59.37	0.0063	2.10	1.016
1.202	2000	57.70	0.0092	2.08	0.930
1.406	2000	91.20	0.0078	3.63	1.914
1.599	2000	150.16	0.007	5.06	2.911

tracking particles for PIV.

The data were captured in and around the clearance gaps as shown in Fig 1(b). The measurement plane for PIV data recording is 20 mm inside from the end face of the lobe. The PIV data were collected at a 45° crank angle where the radial gap is 0.72 mm. The rotor with the stepped shape of the tip, and other clearance dimensions are also indicated in the layout shown in the same Fig. 1(b). The velocity contours obtained by PIV in Fig 2(a) show variation of flow velocities in the gap through the clearance. The magnitude of velocity in the radial clearance gap at rotational speed 1800 rpm is higher than for 2000 rpm as shown in Fig. 2 (b) & (c). The reference measurements for the current study at varied pressure ratios and rotational speeds are given in Table 1.

The experimental setup used variety of sensors to obtain integral performance parameters. Various parameters such as flow, pressure, temperature, torque and power at different pressure ratios and rotational speeds combinations were measured, as shown in Table 2.

2.1.1. PIV data processing

The data processing is divided into three main steps. First step is called pre-processing, which is performed on the images captured to reduce the error brought by incorrect vectors. The background noise is reduced to minimum level by subtracting the minimum intensity obtained by each ensemble of 200 captured images from each individual image. In second step, a coherence-filter based post processing is applied to calculate the raw velocity field using Dantec Dynamic Software as detailed in [43]. The last step is also post-processing, which is performed with the help of Tecplot software [43]. Tecplot is post-processing tool widely used in numerical and experimental analysis. The raw velocity field data from Dantec Dynamic Software is exported to Tecplot for final post-processing in order to obtain contours, extract field parameters by creating lines or points in the flow field, creating vector plots etc. Fig. 2 (a) is the contour obtained from Tecplot and profiles in the Fig. 2(b) are obtained by creating points through the gap in the centre of the gap and across the gap at the exit of the rotor tip where magnitudes of flow field parameters are extracted. For post-processing, the total length of the line for velocity data through and across the gap were kept same for both PIV and CFD. The total number of points on the line through the gap is 30 and across the gap is 25. The start and end point of these two velocity lines (through and across) were kept same for both PIV and CFD. The detailed velocity line position and configuration description is shown in Fig. 16 of Section 3.2.1.

2.2. Numerical modelling of the radial gap flow

In this study, simplified 2D and 3D domains as well as the full 3D fluid domains are considered. Numerical mesh for stationary parts is generated using ANSYS workbench while the deforming rotor domains are meshed with the SCORG rotor grid generator [11]. The flow solver Fluent was used for stationary mesh, dynamic layering and sliding mesh methods, while CFX was used for calculations on the 3D deforming grid. Air is used as a working medium. It is considered an ideal gas with specific heat of 1006.43 J/kg-K, thermal conductivity of 0.0242 W/m-K and viscosity of 1.7894e-05 kg/m-s. The operating parameters shown in Table 1 are used for calculation all cases. Cases modelled in this study are:

- Simplified 2D static numerical mesh
- Simplified 2D moving numerical mesh using unsteady dynamic layering method
- Deforming 3D rotor mesh with filleted tip and hybrid clearances
- Mixture of smoke and air based on the molar weight ratio

2.2.1. Simplified 2D static numerical mesh

This study was performed using a stationary 2D simplified mesh of the Roots blower with a one cell thickness of 5 mm in the direction perpendicular to the 2D domain as shown in Fig. 3(a). In this model, boundary condition on the rotor tip is a no slip moving wall with prescribed angular velocity calculated from the rotor speed and rotor diameter while the casing is stationary. The SST K-omega turbulence model was applied. The inlet and outlet boundary conditions are assigned as pressure inlet and pressure outlet respectively. The side walls have been assigned a symmetric boundary condition. The numerical grid is shown in Fig. 3(b) with the refinements in the boundary layer zone at both casing and rotor tip. This grid has total of 262,959 cells with minimum mesh size of 0.0002 mm and 10 cells in the boundary layer near walls.

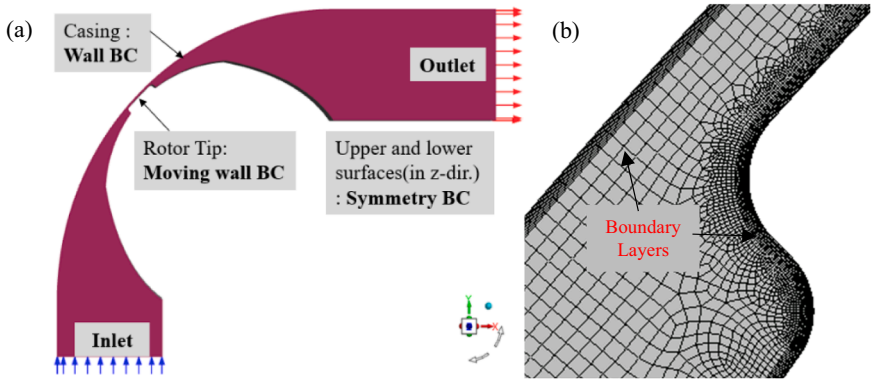

Fig. 3. (a) 2D Simplified computation domain for Steady-state simulation (b) Mesh refinement view.

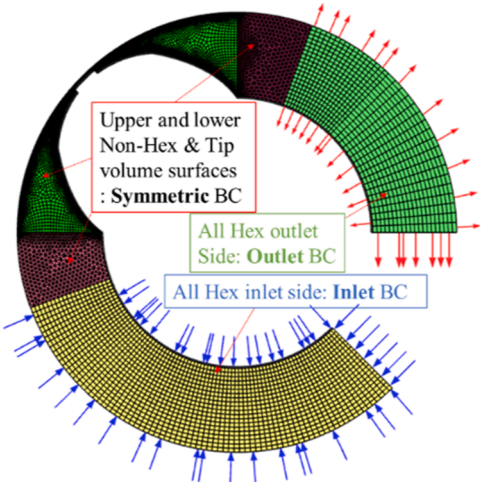

Fig. 4. 2D Simplified computational domain for dynamic layering technique.

2.2.2. *Simplified 2D moving numerical mesh using unsteady dynamic layering*

Dynamic layering technique is a method to generate numerical mesh with moving parts. This meshing method is utilized across various fields such as automotive, turbomachinery and ocean engineering [44]. For modelling rotating parts of the machine, researchers have also been utilizing the moving mesh such sliding mesh method [45]. Daniel et al. [46] adopted this method with Large Eddy Simulation (LES) for modelling vertical axis wind turbine. But in this study of roots blower, dividing a very small gap (100um except at sapphire glass location) into two different fluid zones, one stationary and other rotating, is not very accurate setup to replicate the rotating fluid between solid casing and rotor. However, the Dynamic layering technique sequentially adjusts the movement on boundaries by generating cells at one end and collapsing them on the other end. In this approach, the position of internal nodes is automatically determined based on the specified boundary/object motion, cell type, and meshing schemes. Within prismatic hexahedral and/or wedge mesh zones, dynamic layering is employed to add or remove layers of cells adjacent to boundaries. The dynamic mesh model in ANSYS FLUENT enables the specification of an ideal layer height on the inlet and outlet boundaries, allowing cells adjacent to the inlet and outlet boundaries to be split or merged with the neighbouring layers of cells. This method captures the motion of moving boundary of complex geometries and have better simulation stability. However, the setup can be complex and requires careful consideration of boundary conditions and has higher computational cost. The computational domain and boundary conditions used in this study are shown in Fig. 4. Inlet and Outlet pressure boundary conditions were assigned to inlet and outlet respectively. The upper and lower walls were assigned symmetric boundary conditions. The PISO P-V coupling model [47] and k-omega SST turbulence model were adopted. In order to perform dynamic layering technique, first, the steady-state calculation was carried out to define boundary conditions as shown in Fig. 4. Inlet and outlet boundary walls were not allowed to deform while the immediate fluid volume connected to them were allowed to deform.

2.2.3. *Deforming rotor grid: full 3D fluid domain model*

SCORG is customized grid generation tool used for screw machine, expanders, pumps and motors [8,11]. This tool can produce two different topologies, Rotor-to-casing and Casing-to-rotor. In the first one the whole domain is rotating with the rotor rotation while in the second one the domain remains static and is deformed by the movement of the rotor. In the Rotor-to-casing topology rotor volumes are generated separately and connected via a non-conformal interface. Casing-to-rotor is a single domain structured grid that eliminates the need for non-conformal interface between the rotors.

Application of the casing-to-rotor setup was earlier presented by Singh et al. [25]. However, this topology did not allow to retain the original shape and size of the rotor tip at all time-steps. Therefore, the rotor-to-casing topology is utilised in this work and proved to be more convenient to maintain the size and shape of the tip more accurately, despite the non-conformal interface between domains. The numerical mesh generated using rotor-to-casing topology is shown in Fig. 5(b).

The inlet & outlet were assigned as opening and outlet boundary conditions respectively as shown in Fig. 5(b). As shown in Figs. 5(c) & (d), the generated rotor tip does not fall exactly on the original tip geometry (black line) but it retains its shape in all positions of the rotor. The rotor mesh had 45 radial divisions, 180 angular divisions, 220

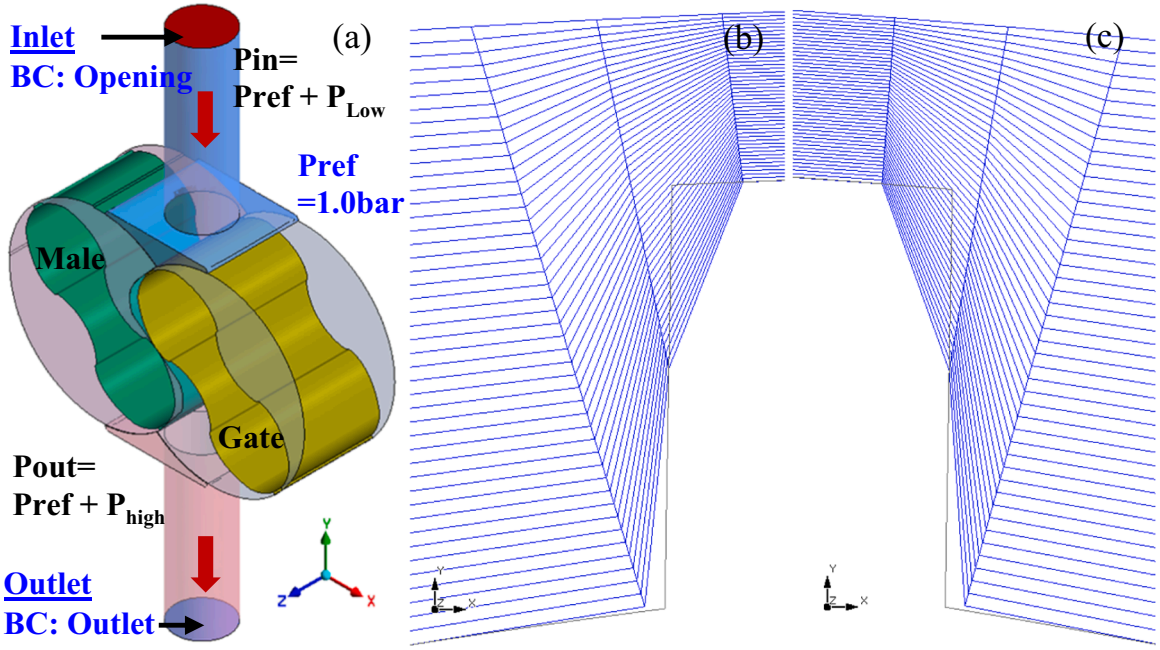

Fig. 5. (a) Computational domain, (b) & (c) Details of the tip on the leading & trailing edge.

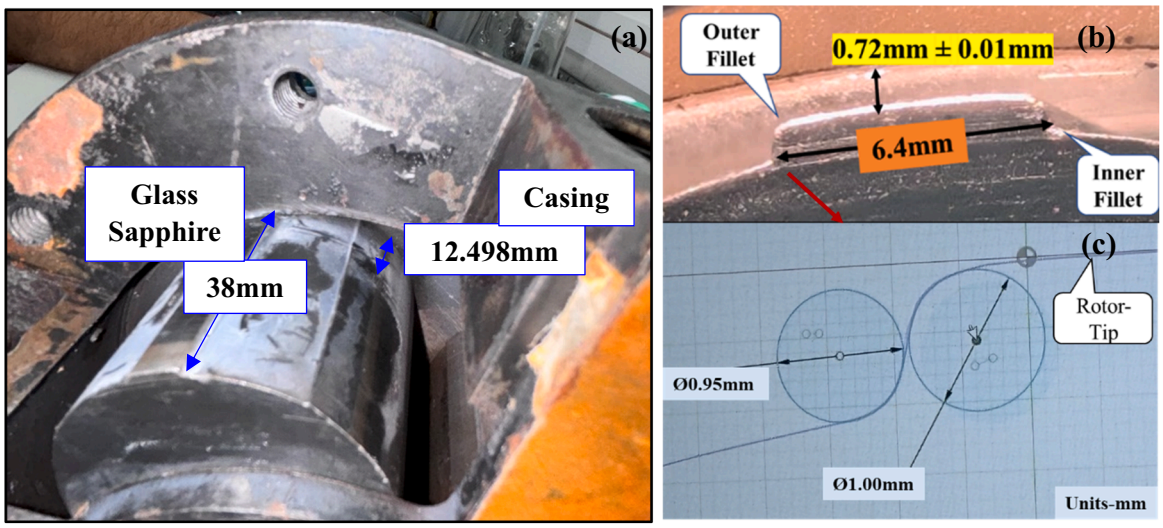

Fig. 6. (a) PIV setup of Roots Blower at Sapphire Glass access, (b) Gap dimension (c) Fillet dimension.

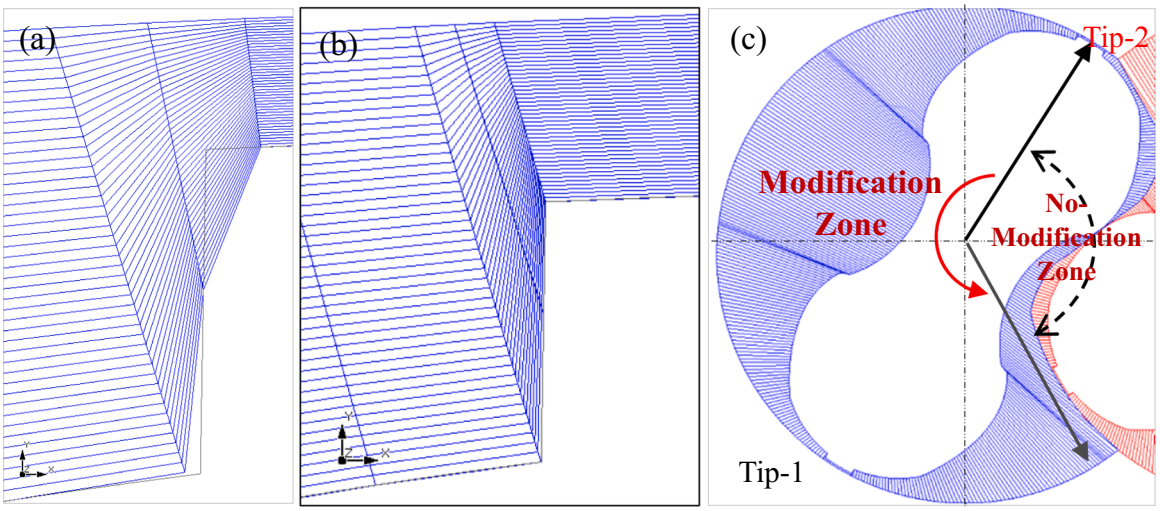

Fig. 7. Detailed mesh of (a) Standard Tip Corner (b) Developed Sharp Tip (c) Grid development area by angle.

circumferential divisions, 65 interlobe divisions and 35 axial divisions. The total number of elements of rotor fluid zone is 1050,000. The radial gap of 0.720 mm in all clearances.

2.3. Deforming 3D rotor mesh with filleted tip and hybrid clearances

The method described above does not represent geometry of the tip accurately since sufficient number of nodes in the tip could not be specified. Therefore, to represent geometry of the leakage gap properly, firstly the fillet radius of the rotor tip was measured using a 3D scanner and the radial gap was measured using filler gauges. Fig. 6(a) is the view of Roots blower section where the glass window is assembled for optical access. Figs. 6(b) and (c) are showing the measured radial gap of 0.72 mm, the tip length of 6.4 mm and fillet radii of R0.45 mm in the root and R0.5 at the tip. The overall length of the Roots blower rotor is 40.498 mm. However, as shown in Fig. 6(a) the glass window covers only 38mmof that length. The clearance between the glass window and the rotor tip is 0.72 mm while the clearance between the casing and rotor tip in all other parts of the Roots blower is 0.1 mm.

2.3.1. Development of the grid to accurately represent the original shape of the rotor tip

Previous research work by Singh et al. [25] using SCORG generated deforming grids was carried out without considering the changes in representation of the shape and size of the rotor tip over the simulation time (Fig. 7(a)). In the present study, a node alignment algorithm was developed to maintain the size of the tip length Fig. 7(b). As the size of the tip through movement of the nodes the rotor tip was maintained, it resulted in reduced quality of the mesh in the calculation domain, and therefore the algorithm was improved further to align the nodes of the casing to maintain the local grid quality. Since the accurate radial leakage flow is required only at the main rotor side, the grid development was limited only to that region while the other rotor tip was not modified. The modification of the male rotor tip was performed only for angles between 60° to 180° as shown in Fig. 7(c)

The new algorithm required to model fillets on the tip is shown in Fig. 8. Steps in the development of the new mesh are explained in the flow chart in Fig. 9. The procedure to accurately represent the fillet shape increased the total number of the grid points on the rotor. The same number of nodes were inserted on the casing. To improve quality of the mesh, the distribution of nodes between the rotor and casing boundary was modified.

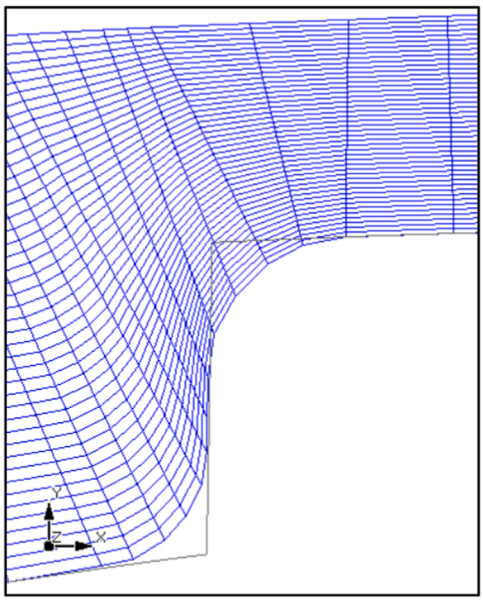

Fig. 8. Detailed mesh of Fillet tip.

2.3.2. Development of the mesh with hybrid clearances

The procedure for representing two different clearances, one in the area of the glass window and the other of the original casing is shown in Fig. 10. The algorithm starts with generating the first numerical mesh for the clearance of 0.1 mm and replacing nodes in the area of the glass window with clearance of 0.72 mm.

The resultant 3D geometry with hybrid clearances is shown in Fig. 11 (a). Numerical meshes for the flow domain around the main and gate rotors are separately created and connected through the non-conformal interface. Additionally, one set of grids for the main and gate rotors was created of the length of 38 mm covered by the glass window with the clearance between the main rotor and casing of 0.72 mm. Another set of grids was generated for the remaining length of 12.498 mm and clearances of 0.1 mm. These two sets of grids which represent fluid domain of the main rotor were connected through a non-conformal interface as shown in Fig. 11(b). Figs. 11(c) and 11(d) show that variable radial gap in the region of the glass window. In addition to the radial and interlobe clearance gaps which are inherent part of the numerical mesh generated with SCORG, axial gap of 0.07 mm was added as an additional domain on both sides of the rotor end faces.

2.4. Mixture of smoke and air

The PIV test requires seeding of the flow with particles which are tracked to determine flow velocity in clearances. The n-Octanol liquid was used to generate smoke for the test. The amount of injected smoke changes density of the air and smoke mixture and it is necessary to investigate the influence on flow simulation results. The properties of air and smoke are listed in Table 3. The study considered two concentrations of smoke in air; 5 % and 15 %.

Since in the current study, a single-phase flow has been solved with the density of an ideal gas, Eq. (1) is applied to the molecular weight of air and smoke to get an equivalent mixture molecular weight.

$$\rho_m = \sum_{\alpha} \rho_\alpha r_\alpha \tag{1}$$

where, ρ_m is the mixture molecular weight, ρ_α is the material molecular weight and r_α is volume fraction.

The corresponding molecular weights of the mixture for cases modelled here are 35 g/mol for 5 % and 45 g/mol for 15 % smoke concentration in the mixture.

3. Results and discussion

The numerical results of velocity field, discharge flow and temperature are compared against the experimental data. Velocity contours and profiles are compared with PIV results while the discharge flow and temperature are compared with the experimental results given in Table 2. For the verification of the Full 3D model, discharge mass flow rate and temperature are compared with measured values. The test results are averaged over running time of approximately 15 mins. Similarly, numerical results are averaged across the 10 cycles of rotation.

3.1. Velocity magnitude in clearances

This section compares the flow pattern through and across radial clearance gap as shown in Fig. 16 considering velocity magnitude obtained at different rotational speeds and pressure ratios. The results of PIV measurements from literature [41] were used to compare the velocity field obtained by simulation with the experiment. The flow field of simplified CFD models is compared with the PIV results for the test conditions listed in Table 1. The results of velocity profile are compared at 45° crank angle of the main rotor.

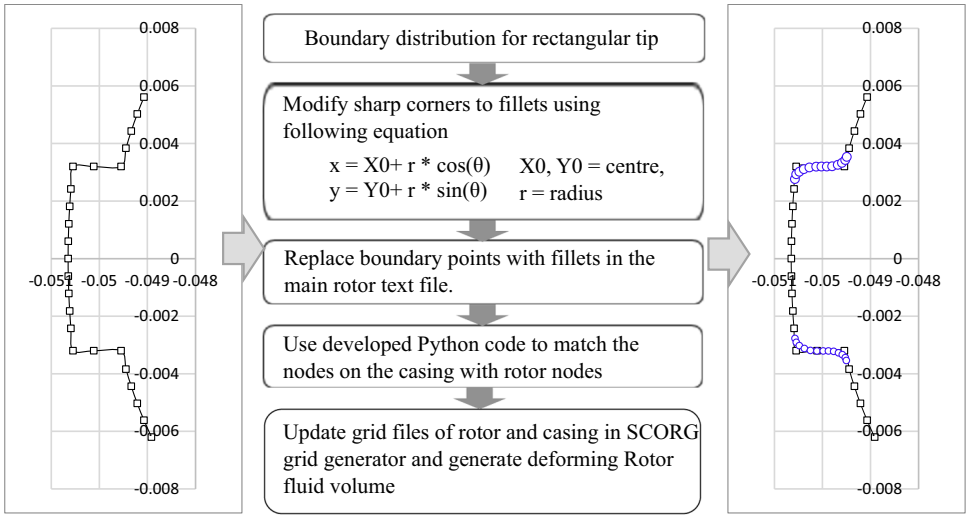

Fig. 9. Flow chart of development stages from sharp corner (left) to fillet (right).

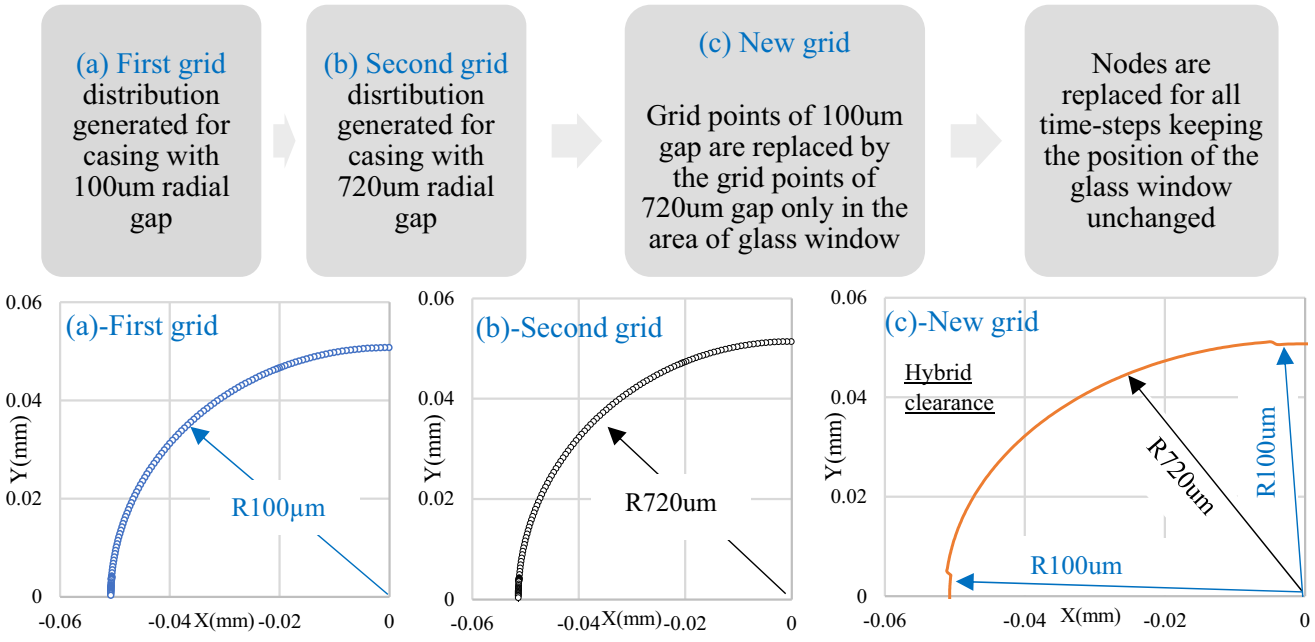

Fig. 10. Flow chart of development stages to represent Sapphire Glass.

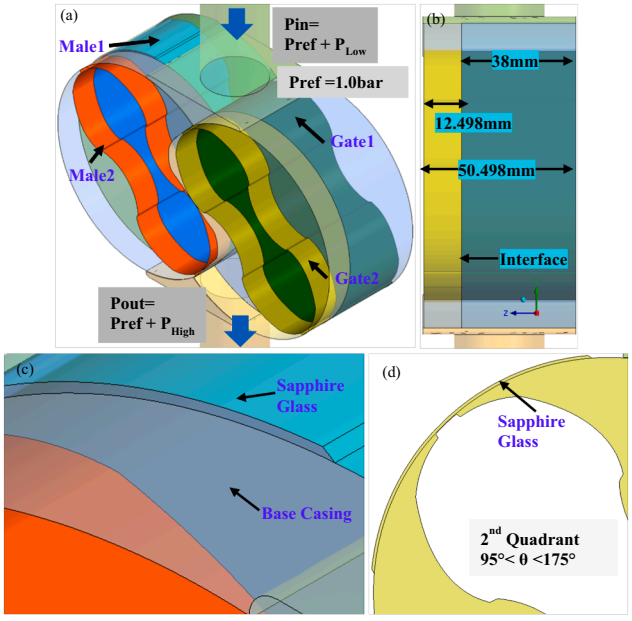

Fig. 11. (a) 3D model with hybrid gaps, (b) Rotor volumes connected via an interface, (c) Closer view of the mesh with hybrid clearances, (d) Sapphire glass covering 80° in 2nd quadrant of the Roots blower.

Table 3
Fluid Properties.

Property (at 25 °C)	Air	Smoke/n-Octanol
Composition	N2(78 %) + O2(22 %)	$CH_3(CH_2)_6CH_2OH$
Molecular Weight (ρ_a)	28.97 g/mol	130.23 g/mol
Density	1.225 kg/m³	820 kg/m³
Specific Heat Capacity (Cp)	1.005 kJ/kg·K	2.0 kJ/kg·K
Dynamic Viscosity (µ)	1.831e-5 Pa-s	7.31e-3Pa-s

3.1.1. *Velocity magnitude for simplified 2D schemes*

The calculated velocity field with two 2D simplified schemes, namely static mesh with moving wall boundary condition and dynamic layering mesh at two different pressure ratios of 1.6 and 1.2 and three different rotational speeds of 1500, 1800 and 2000 RPM was compared with PIV results. Fig. 12 shows the comparison of velocity contours at pressure ratio of 1.6 and 2000 RPM. The comparison shows modelling conditions with no-smoke and 5 % smoke. In the case with no smoke, both modelling techniques resulted with higher velocity magnitude than PIV as shown in Fig. 12(b) and (c). The case of 5 % smoke showed better agreement with PIV test as shown in Fig. 12(d) and (e). The dynamic layering technique with 5 % concentration of smoke in air has shown more variation in velocity gradient through the gap which better agrees with measured results. This technique is more suitable for modelling of the gap flow using simplified 2D methods.

The velocity contours for other pressure ratios and rotational speeds and smoke concentration of 5 % are shown in Fig. 13. The velocity gradients at the tip-exit are more pronounced for the dynamic layering (Fig. 13(3)) than for the static mesh (Fig. 13(2)) due to the rotational effect of the moving mesh. The dynamic layering (Fig. 13(3)) has also more accurately captured the physics of flow at the tip entrance. Results indicate that the leakage flow is sensitive to the speed of the rotor. It is expected that the accuracy of modelling could be improves with the full 3D numerical mesh.

3.1.2. *Velocity magnitude for the 3D model with filleted tip and hybrid clearances*

This section discusses velocity magnitude obtained by the full 3D model of the Roots Blower with improvements for representing filleted tip and hybrid clearances. The comparison of velocity magnitudes obtained using this 3D mesh with the PIV test results is shown in Fig. 14 for pressure ratio 1.6 and speed of 2000 RPM. The model considers all gaps including hybrid radial gap (0.72 mm and 0.1 mm), interlobe gap of 0.1 mm and the axial gap varied from 0.07 mm to 0.08 mm as well as seeding with 0 %, 5 % and 15 % of smoke in air. The velocity magnitude for the case without seeding shown in Fig. 14(b) shows velocity magnitudes higher than in measurements. The 15 % smoke seeding significantly decreased the velocity magnitude throughout the clearance because of the high density of the mixture as shown in Fig. 14(c). The

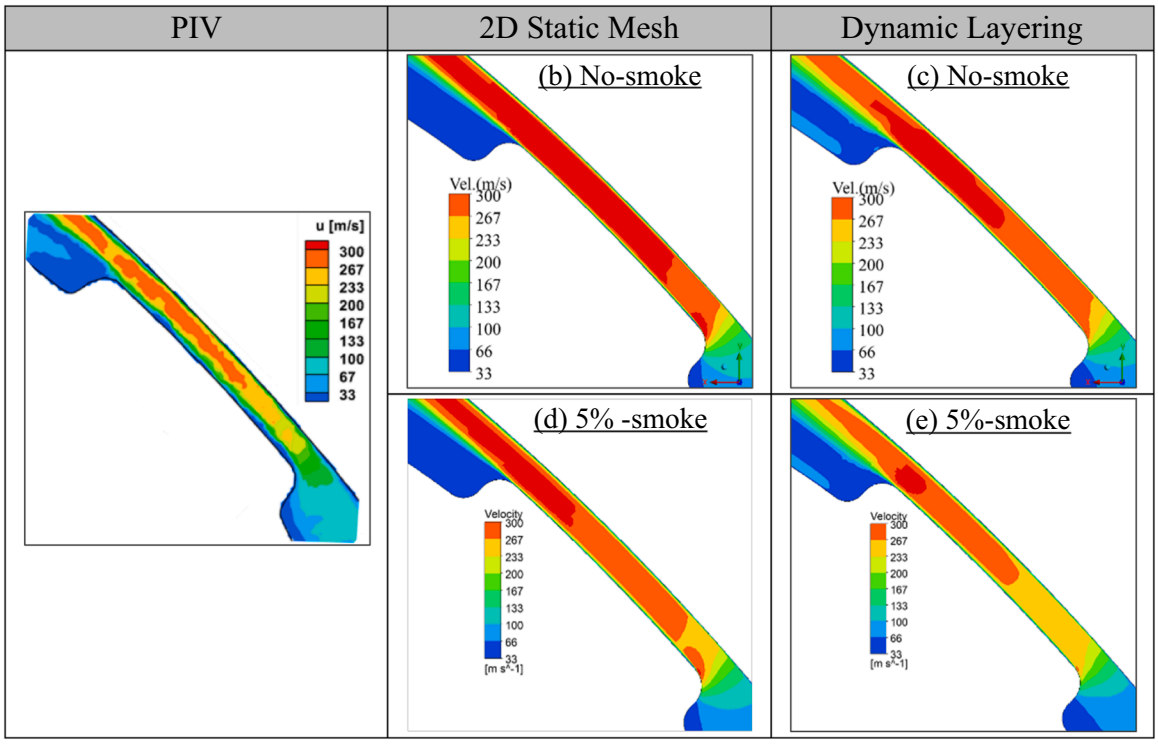

Fig. 12. Comparison of velocity contours of PIV, Static mesh- Moving Wall BC and Dynamic Layering at PR1.6 & 2000 RPM.

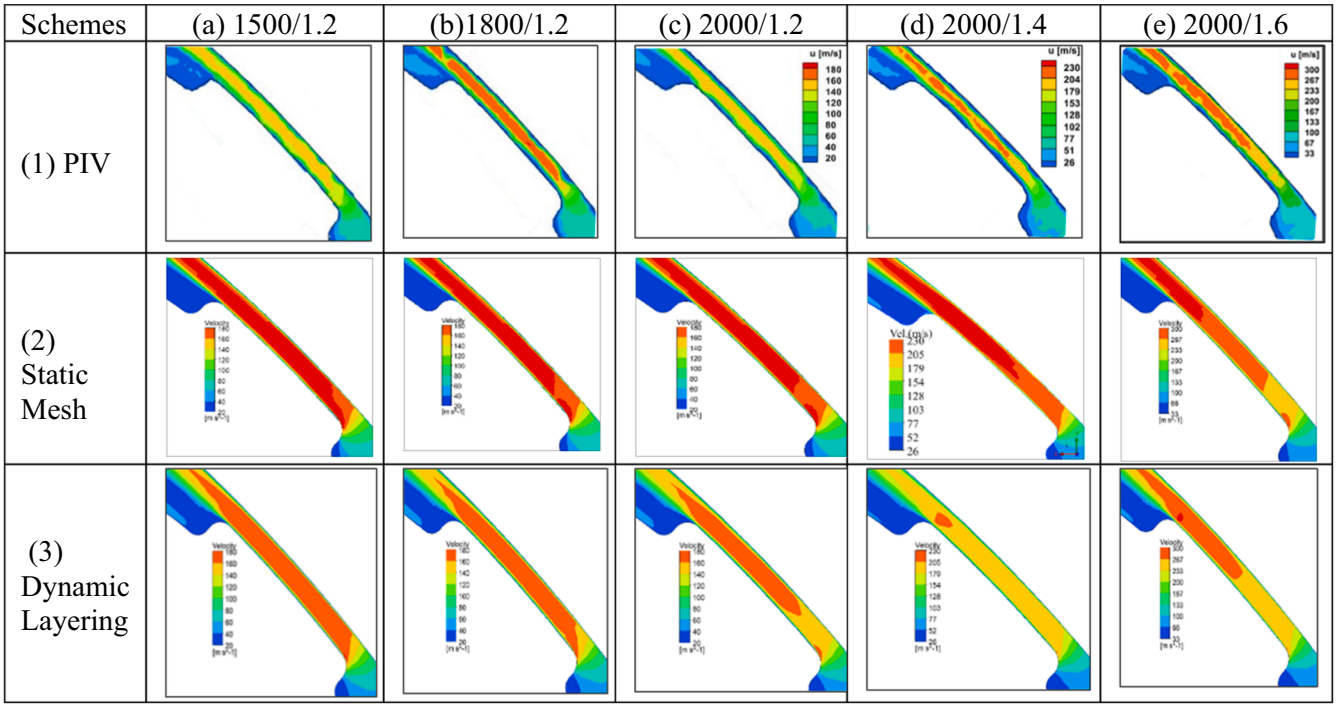

Fig. 13. Velocity contours comparison for (1) PIV, (2) for Static mesh and (3) for Dynamic Layering mesh.

case with 5 % smoke seeding and 0.07 mm axial gap produces improved velocity magnitude and is closer to PIV as shown in the Fig. 14(d). The result of axial gap 80 μm and 5 % smoke seeding has similar velocity magnitude as in the case of 70 μm but produces more variation in the velocity magnitude in clearances.

Fig. 15 shows deviation between the calculated and test results of velocity magnitudes in the middle of the clearance gap. The X value in mm is the distance from the tip entry point. The 3D model with rounded tip, hybrid clearances, 70 μm axial gap and 5 % smoke is closest to the measured results with <5 % deviation.

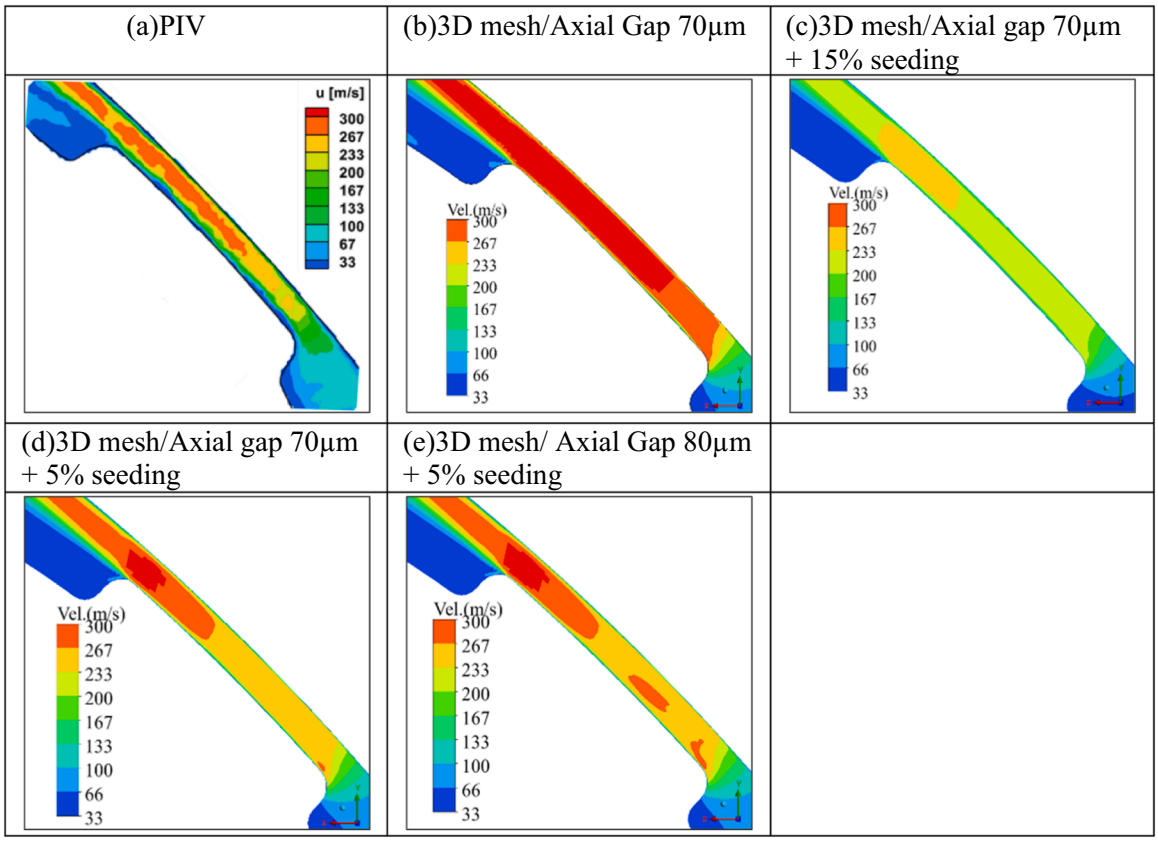

Fig. 14. Velocity contours at different 1.6 PR and 2000 RPM.

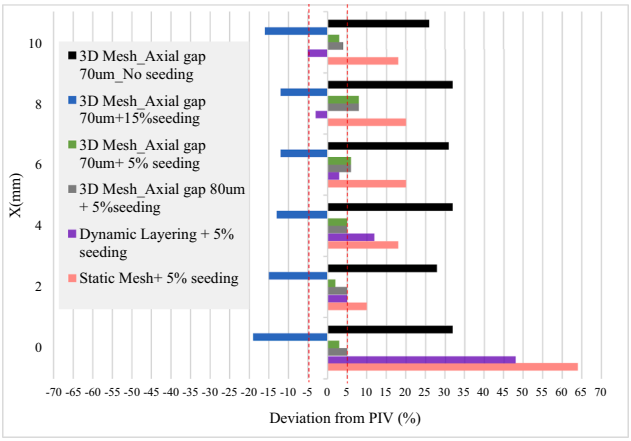

Fig. 15. Velocity magnitude deviation from the PIV measurement at pressure ratio 1.6 and 2000RPM (the ordinate value X represents the location through the gap as shown in Fig. 17 of next section).

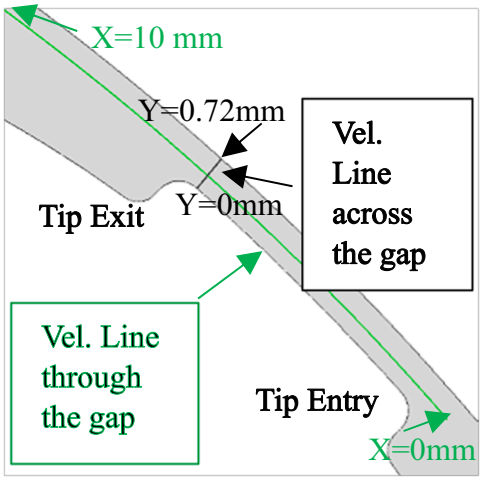

Fig. 16. Velocity lines indication in clearance gap for obtaining velocity profiles with corresponding start and end values of X; black color for across gap line and green color for through gap line.

3.2. *Velocity profile, flow rate and temperature in clearance gaps*

3.2.1. *Velocity profiles in clearance gap*

Fig. 17 shows comparison of the velocity profiles of all considered numerical schemes with PIV test results. Lines alongside which the velocity profiles are compared through and across the gap are displayed in Fig. 16.

The velocity profile at the pressure ratio 1.6 and speed of 2000 rpm, for all schemes is compared through the gap as shown in Fig. 17(a) and across the gap as shown in Fig. 17(b). All simulations show more changes in flow gradients though the gap than what is observed by PIV. Stationary mesh with the moving wall boundary and 5 % seeding shows higher velocity magnitude in comparison to the other methods. The dynamic layering technique produces higher velocity at the tip-entry similar to the stationary mesh but the velocity profile in the clearance gap and at the tip exit is closer to the PIV results, as shown in Fig. 17(a). The 3D model with hybrid clearances and smoke seeding have shown improved velocity profile and magnitude through the clearance from the tip-entry to tip-exit. The mesh with 70 µm axial gap and 5 % smoke seeding is in the best agreement with PIV measurements. All numerical models have shown tendency towards higher velocity at tip-entry than

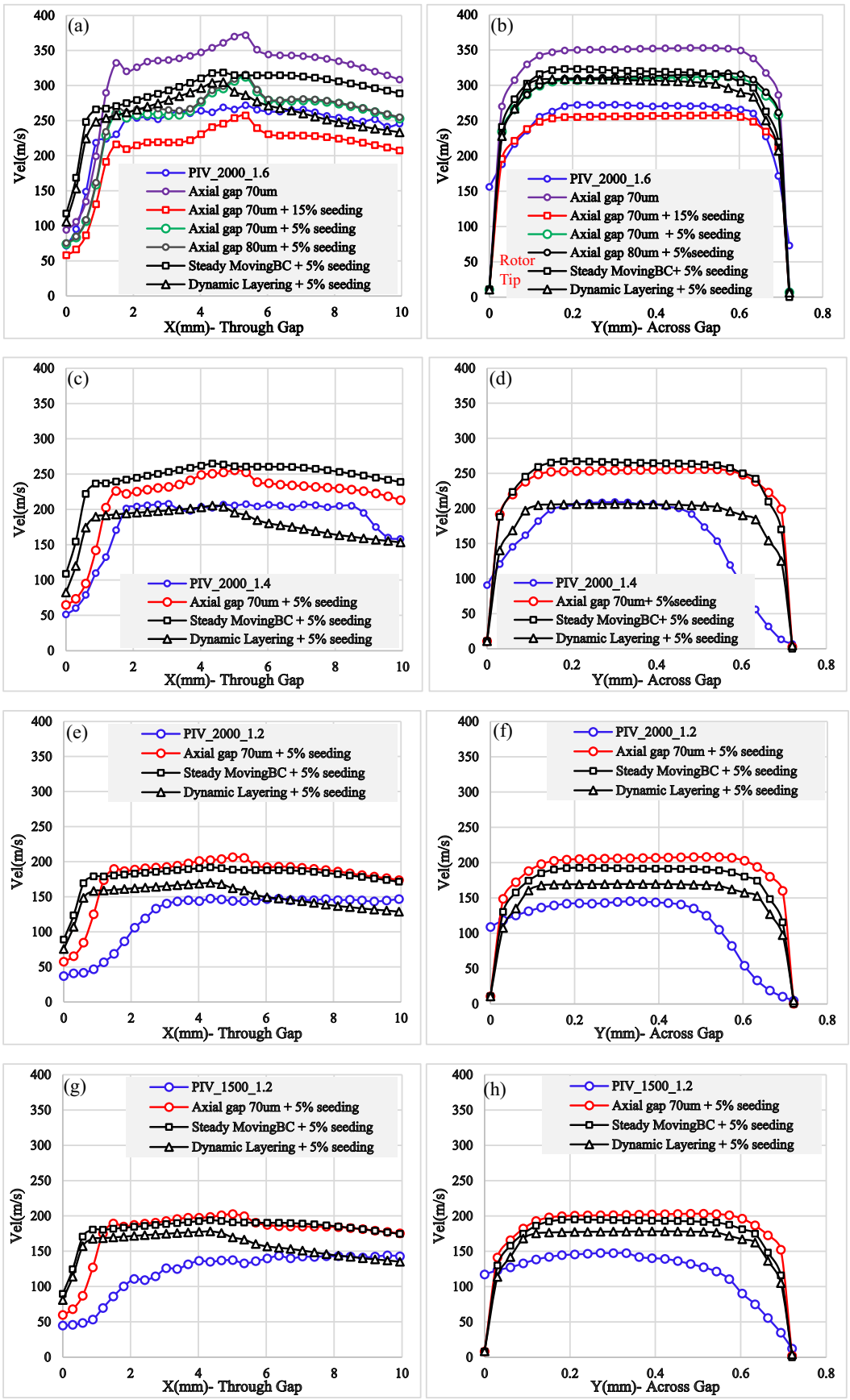

Fig. 17. Comparison graph of velocity profiles (a) & (b), (c) & (d), (e) & (f) and (g) & (h)- through & across at PR1.6/2000, PR1.4/2000, PR1.2/2000 and PR1.2/1500 respectively.

Table 4
Discharge Flow Rate & Temperature comparison of 3D mesh models.

Conditions	Cases	Discharge Flow Rate		Discharge Temperature	
		$\dot{m}$ (kg/m)	%Δ	T (°C)	%Δ
PR1.6/ RPM2000	Test	0.420		150.1	
	Axial gap 70μm	0.492	17.1 %	132.0	−12.1 %
	Axial gap 70 μm + 15 % seeding	0.798	90.0 %	93.0	−38.1 %
	Axial gap 70 μm + 5 % seeding	0.498	18.6 %	129.7	−13.6 %
	Axial gap 80 μm + 5 % seeding	0.447	6.4 %	140.0	−6.8 %

what is observed with PIV. However, the velocity profile across the gap shown in Fig. 17(b) indicates that 15 % smoke seeding results are closer to PIV which is contradictory with the pattern of the velocity profile through the gap. With numerical models it was possible to obtain velocity values at the wall and its vicinity. However, due to reflection, with PIV measurements it was not possible to obtain velocity values near walls. It is observed that the flow pattern across the gap for numerical models and PIV measurements show the same trend. The flow propagation in the direction of fluid movement is higher for cases without smoke seeding.

At pressure ratios of 1.2 and 1.4, only the smoke seeding concentration or 5 % was considered. Velocity profiles for the pressure ratio of 1.4 and speed of 2000 RPM are shown in Fig. 17(c) and (d). The velocity profile in the clearance gap obtained by the dynamic layering technique is matching well with PIV. However, it deviates significantly at the tip-entrance and the tip-exit. 3D mesh with hybrid clearances shows good agreement in all three zones of the tip-entry, tip-clearance and tip-exit. The across velocity profile shown in Fig. 17(d) indicated that the dynamic layering is in the best agreement with the test results in the clearance region.

At the lowest pressure ratio of 1.2 and speeds of 2000 and 1500 shown in Fig. 17(e) - (f) and (g)-(h) respectively, the dynamic layering technique has shown better agreement with PIV than the stationary mesh and 3D mesh with hybrid clearances. At these conditions, the velocity profile is not much affected by rotational speed. It is reasonable to say that numerical models are in good agreement with PIV test results.

3.2.2. *Discharge flow rate and temperature*

This section is dedicated to the comparison of the integral flow and temperature data. The integral parameters in the experimental results are recorded at steady state conditions after sufficient time for all parameters to stabilise. The results of the numerical model with the 3D numerical mesh, are averaged over 10 cycles of rotation. At the speed of 2000 and pressure ratio of 1.6, the discharge flow rate and temperature obtained with the 3D model with axial gap of 80 μm and 5 % seeding is showing good agreement with the test as shown in Table 4. The 3D model with 70 μm axial gap and 5 % seeding has shown higher deviation from the test but is well within the acceptable range. However, in all 3D modelling schemes, the mass flow is overestimated, and temperature is underestimated. It is possible to make some adjustments by changing the size of the gate rotor radial gap [26]. However, it is assumed that this is not required for this study as it focuses on the leakage flow for which deviations were found to be within the acceptable level.

In case of positive displacement compressor models such as roots blower, a highly deforming mesh is required in the rotor domain. The performance estimated from these models namely mass flow rate and indicated power is dependent on the accuracy of velocity, pressure and temperature field. In actual working condition, the gaps between the rotor and housing vary to a certain extent. In the current study, these gaps have been fixed as demanded by the CFD model. However, using test data their values have been calibrated as indicated in Table 4 using axial gap.

3.3. *Pressure, density and temperature distribution*

In this section, pressure, density and temperature variations will be analysed. The comparison is made for 5 % seeding in both simplified models and 3D models with 70 μm and 80 μm axial gap. Fig. 18 shows the comparison of the pressure field of all numerical schemes at pressure ratio of 1.6 and speed of 2000 RPM. The pressure drop across the tip is 105 kPa for static mesh, 71.82 kPa for dynamic layering, 59.8 kPa for 3D

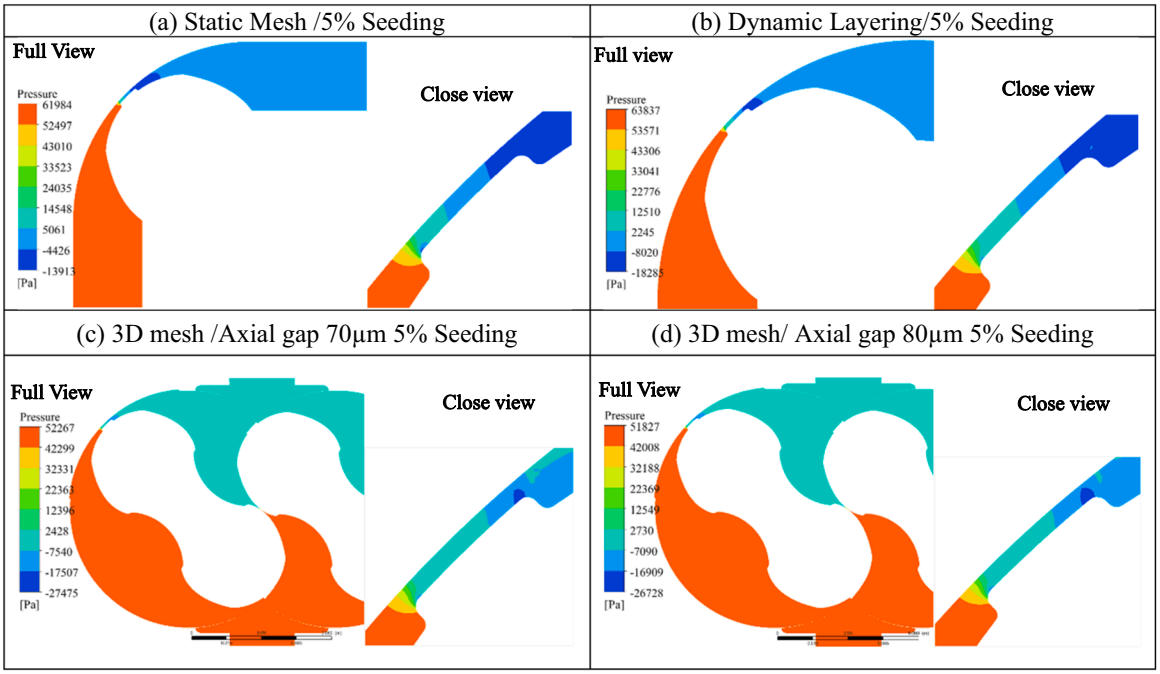

Fig. 18. Pressure contours at pressure ratio 1.6 and speed 2000 RPM.

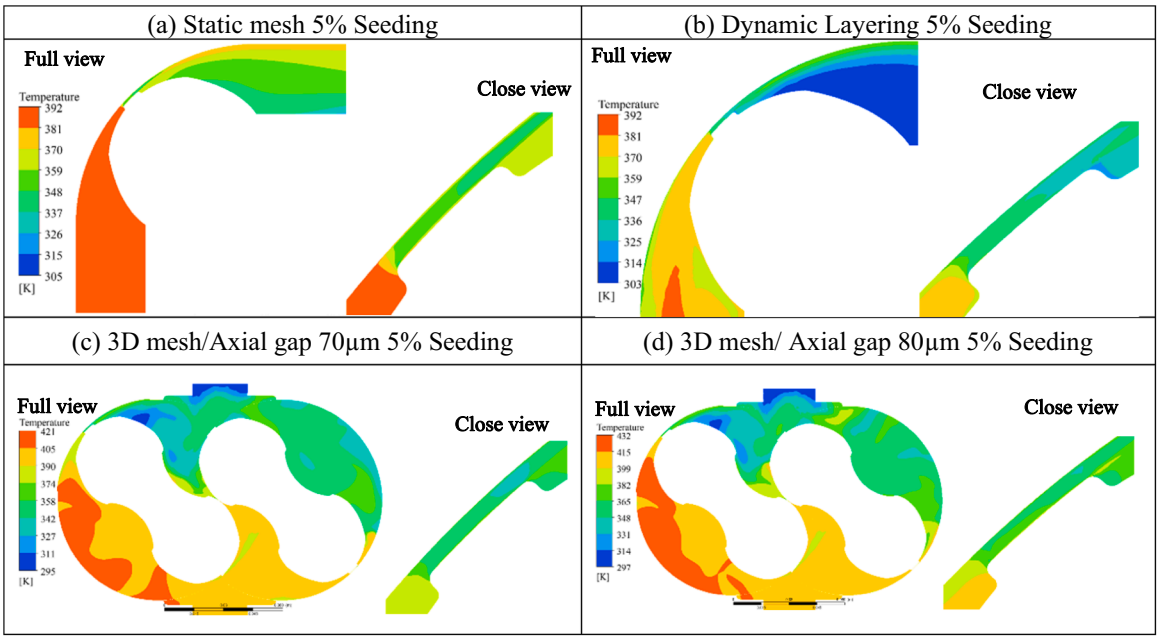

Fig. 19. Temperature contour comparison at PR1.6 and 2000 RPM.

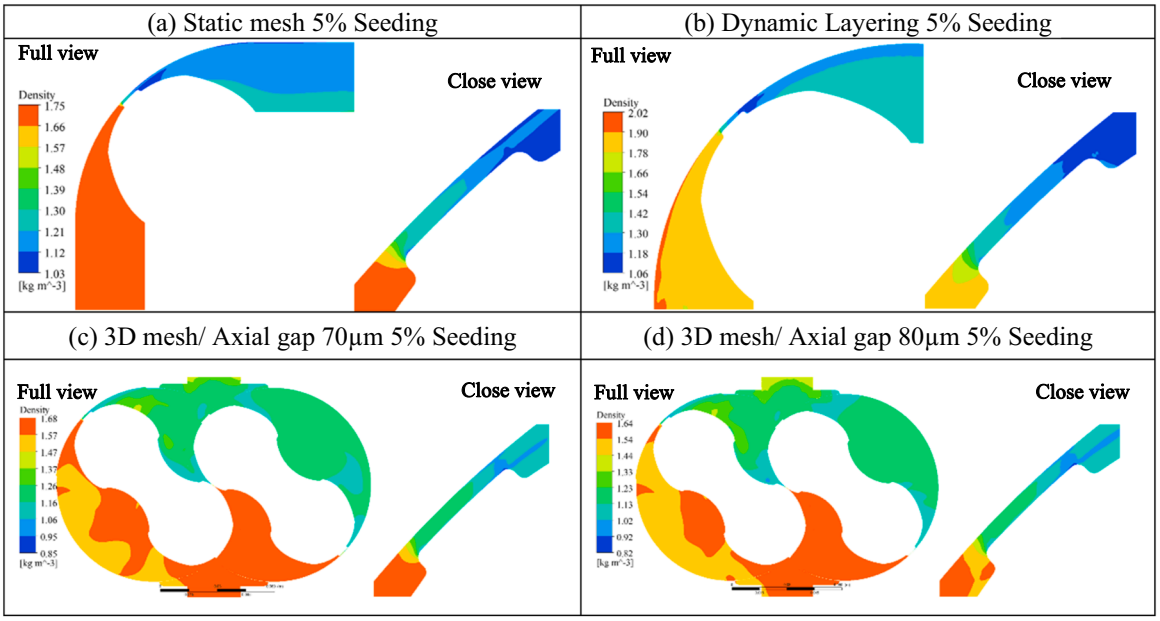

Fig. 20. Density contour comparison at pressure ratio 1.6 and speed 2000 RPM.

mesh with 70 μm axial gap and 61.91 Pa for 3D mesh with 80 μm axial gap. The pressure difference is higher for simplified models than for the 3D mesh with hybrid clearances. Simplified models therefore have higher values of velocity in the clearance gap.

Fig. 19 is the comparison of the temperature profile among all the numerical schemes. Temperature difference across the tip is 51.7 °C for static mesh, 44 °C for dynamic layering, 45.2 °C for 3D mesh with 70 μm axial gap and 49.55 °C for 3D mesh with 80 μm axial gap. The maximum temperature difference was observed in the static mesh and the lowest is in the dynamic layering mesh.

Fig. 20 shows the comparison of the density contours for used numerical schemes. The density recorded in the centre point between the tip entrance and tip exit is 1.25 kg/m^3 for static mesh, 1.28 kg/m^3 for dynamic layering mesh, 1.23 kg/m^3 for the 3D mesh with 70 μm axial clearance and 1.24 kg/m^3 for the 3D mesh with 80 μm axial clearance. The variation of density in the leakage gap across the used methods is negligible.

Table 5. shows the summary of all numerical schemes applied in this study. The 3D mesh with hybrid clearances produces results closest to the experiment and has shown better sensitivity to the rotational speed of the rotor.

4. Conclusion

This work has presented the validation of numerical model for radial leakage flow in roots blower using PIV experimental data. Numerical study utilized and compared three approaches, namely the 2D simplified static mesh with the moving wall boundary, unsteady dynamic layering

Table 5
Summary of numerical schemes.

Criteria	Simplified 2D Methods		Advanced 3D Methods
	Static Mesh	Dynamic Layering	Hybrid Clearances
Description	- Steady state - Moving wall boundary conditions - Rotor tip Tangential velocity	- Unsteady state - Grid moves in the flow field - Time step - per 0.1° rotation	- 3D Deforming rotor grid - Unsteady, Full rotation of rotors. - Hybrid clearance method to represent two different radial clearances.
Numerical Aspects	- Modelling is easy - Total simulation time is approx. 25mins	- Relatively complex modelling. - Total simulation time is approx. 600mins	- 3D representation of the model. - Grid generation and Calculation is carried out on different solvers. - Total simulation takes around 4800 mins
Velocity magnitude	- Velocity field is affected by the speed of the rotor but has higher magnitude than the test		-Velocity field is significantly affected by speed of the Rotor and closer to test
Velocity Plots	-Higher deviation at tip-entry and at high PR		-Lower deviation at high PR but higher deviation at lower PR
Accuracy	- Less accurate - Based on modelling assumptions.	- Accuracy depends on smoothness of addition and removal of mesh layer.	- Highly accurate since it completely replicates the geometry of the fluid domain
Sensitivity	- Flow is sensitive to the rotational speed.		
Ability	- Limited to leakage flow		- Main flow, leakage flow as well as power can be estimated
Limitation	-Instantaneous flow field are primarily captured. -Discharge flow and temperature cannot be measured.		- Deviation in the leakage flow is dependent on the gap size.

mesh technique and the 3D deforming rotor grid technique. The Deforming grid model was found to be more accurate as it replicated the features of rotor profile with rotating motion. Further, the 3D deforming grid was improved by developing a grid for filleted tip and implementing hybrid clearances to mimic the physical geometry. Also, the fluid composition was changed by interpolating between molar weights of air and smoke to capture the effect of smoke seeding. The study was performed with 5 % and 15 % concentration of smoke. Axial gap in 3D model was varied from 70 μm to 80 μm. The numerical schemes were compared with experimental data considering velocity field, discharge flow and discharge temperature.

Numerical results indicate that the gap flow field is sensitive to the rotational speed of rotors, similar to what was observed through the PIV experiment. It was noticed that influence of the rotor speed on the flow field is higher for the higher-pressure ratios than for the low-pressure ratios. Numerical schemes without smoke seeding have shown on average 80m/s higher peak velocity compared to the test results. Conversely, smoke seeding has shown significant improvement in the gap flow profile. The deviation of the velocity field for the 3D mesh, with 5 % smoke seeding and 70 μm axial gap is found to be well within the 5 % range when compared to the PIV measurements. With an axial gap of 80 μm, with 5 % smoke the discharge flow rate and temperature was closest to the measured data, but velocity was found to be slightly higher by about 1 % near the tip inlet. The modelling procedures presented in this research can be adopted to twin screw compressors and other positive displacement machines.

CRediT authorship contribution statement

Neeraj Bikramaditya: Writing – review & editing, Writing – original draft, Formal analysis, Data curation. **Sham Rane:** Writing – review & editing, Writing – original draft, Methodology, Formal analysis, Conceptualization. **Ahmed Kovačević:** Writing – review & editing, Writing – original draft, Formal analysis, Conceptualization. **Mohammad Omidyeganeh:** Supervision, Conceptualization.

CRediT authorship contribution statement

Neeraj Bikramaditya: Writing – review & editing, Writing – original draft, Formal analysis, Data curation. **Sham Rane:** Writing – review & editing, Writing – original draft, Methodology, Formal analysis, Conceptualization. **Ahmed Kovačević:** Writing – review & editing, Writing – original draft, Formal analysis, Conceptualization. **Mohammad Omidyeganeh:** Supervision, Conceptualization.

Declaration of competing interest

The authors declare that they have no known competing financial interests or personal relationships that could have appeared to influence the work reported in this paper.

Acknowledgements

This research is financially supported by the Centre for Compressor Technology at City, St. George's University of London and Howden Compressor. The authors acknowledge City, St. George's University of London for the help provided and granted permission for the HPC (high-performance computing) facility.

Data availability

Data will be made available on request.

References

[1] D. Vittorini, G. Bianchi, R. Cipollone, Energy saving potential in existing volumetric rotary compressors, Energy Procedia 81 (2015) 1121–1130, https://doi.org/10.1016/j.egypro.2015.12.137.
[2] Yi Zhang, X. Qiao, The current status and future development trends of oil-free compressor, in: IOP Conf. Series: Journal of Physics: Conf. Series 1303, 2019 012045, https://doi.org/10.1088/1742-6596/1303/1/012045.
[3] A. Kovacevic, N. Stosic, I.K. Smith, A numerical study of fluid-solid interaction in screw compressors, International Journal of Computer Applications in Technology (IJCAT) 21 (4) (2004) 148–158, https://doi.org/10.1504/IJCAT.2004.006651, 2004.
[4] A. Kovacevic, S. Rane, N. Stosic, Computational fluid dynamics in rotary positive displacement screw machines, in: 16th International Symposium on Transport Phenomena and Dynamics of Rotating Machinery, Apr 2016. Honolulu, United States. ffhal-01879361, https://hal.science/hal-01879361v1.
[5] A. Kovacevic, S. Rane, Challenges in 3D CFD modelling of rotary positive displacement machines, Journal of Physics conference (2021), https://doi.org/10.1088/1742-6596/1909/1/012063.
[6] A. Kovacevic, S. Rane, N. Stosic, Yu Jiang, S.;. Lowry, M. Furmanczyk, Influence of approaches in CFD solvers on performance prediction in screw compressors, in: International Compressor Engineering Conference. Paper 2252, 2014. https://docs.lib.purdue.edu/icec/2252.
[7] S. Rane, A. Kovacevic, N. Stosic, M. Kethidi, Grid deformation strategies for CFD analysis of screw compressors, City University London, Centre for Positive Displacement Compressor Technology, London International Journal of Refrigeration 36 (2013), https://doi.org/10.1016/j.ijrefrig.2013.04.008.
[8] S. Rane and A. Kovacevic, "Algebraic generation of single domain computational grid for twin screw machines" Part I. Implementation Advances in Engineering Software 107 38–50, https://doi.org/10.1016/j.advengsoft.2017.02.003.
[9] S. Rane and A. Kovacevic, "Algebraic generation of single domain computational grid for twin screw machines" Part II – Validation Advances in Engineering Software 109 31–43, https://doi.org/10.1016/j.advengsoft.2017.03.001.

[10] A. Kovačević, N. Stošić, IK. Smith, GRID ASPECTS OF SCREW COMPRESSOR FLOW CALCULATIONS, ASME Congress, Orlando, Florida, 2000, https://doi.org/10.1115/IMECE2000-1300, 05-10 November.
[11] A. Kovacevic, Three-Dimensional Numerical Analysis For Flow Prediction in Positive Displacement Screw Machines, School of Engineering and Mathematical Sciences, City University London, UK., 2002. Ph.D. Thesis, https://openaccess.city.ac.uk/id/eprint/7604/.
[12] F. Ye, G. Bianchi, S. Rane, SA. Tassou, J. Deng, Numerical methodology and CFD simulations of a rotary vane energy recovery device for seawater reverse osmosis desalination systems, Appl. Therm. Eng. 190 (2021) 116788, https://doi.org/10.1016/j.applthermaleng.2021.116788.
[13] F. Ye, G. Bianchi, S. Rane, SA. Tassou, J. Deng, Analytical grid generation and numerical assessment of tip leakage flows in sliding vane rotary machines, Advances in Engineering Software 159 (2021) 103030, https://doi.org/10.1016/j.advengsoft.2021.103030.
[14] N. Bikramaditya, S. Rane, A. Kovacevic, B. Patel, "CFD analysis of leakage flow in radial tip gap of roots blower", 13th International Conference on Compressors and Their Systems, DOI: 10.1007/978-3-031-42663-6_4.
[15] D. Rowinski, A. Nikolov, A. Brümmer, Evaluation of cut cell cartesian method for simulation of a hook and claw type hydrogen pump, IOP Conf. Series: Materials Science and Engineering 425 (2018) 012019, https://doi.org/10.1088/1757-899X/425/1/012019.
[16] Y. Lu, S. Rane, A. Kovacevic, Numerical modelling of hook and claw-type vacuum pump performance based on cut cell cartesian method, Int. J. Hydrogen. Energy 47 (2022), https://doi.org/10.1016/j.ijhydene.2022.05.110, 23006 e23018.
[17] K. Theofanidis, Y. Lu, A. Kovacevic, et al., CFD analysis on the effect of discharge port geometry of the hook and claw vacuum pumps, in: K. Theofanidis, et al. (Eds.), IOP Conf. Ser.: Mater. Sci. Eng. 1180 012063DOI, 2021, https://doi.org/10.1088/1757-899X/1180/1/012063.
[18] M. Tutar, C. Emre Üstün, H. Mutlu, A thermodynamic computational model analysis of a newly designed Tri-Rotor (T-R) volume air compressor, Thermal Science and Engineering Progress 53 (2024) 102708, https://doi.org/10.1016/j.tsep.2024.102708.
[19] K. Ma, B. Guo, Y. Zhou, Y.B. Wang, et al., CFD simulation and experimental studying of a dry screw vacuum pump, in: K. Ma, et al. (Eds.), IOP Conf. Ser.: Mater. Sci. Eng. 1180 012043, 2021, https://doi.org/10.1088/1757-899X/1180/1/012043.
[20] P.K. Kauder and D.D. Stratmann, "Theoretical gas flow through gaps in screw-type machines," 2002.
[21] J. Vimmr and O. Fryč, "Numerical simulation of leakage flow between moving rotor and housing of screw compressor.".
[22] S.H. Sun, A. Kovacevic, C. Bruecker, A. Leto, G. Singh, M. Ghavami, Numerical and experimental analysis of transient flow in roots blower, IOP Conf. Series: Materials Science and Engineering 425 (2018) 012024, https://doi.org/10.1088/1757-899X/425/1/012024.
[23] S.K. Sun, B. Zhao, X.H. Jia a.nd X.Y. Peng, ."Three-dimensional numerical simulation and experimental validation of flows in working chambers and inlet/outlet pockets of Roots pump Vacuum" 137 195–204, https://doi.org/10.1016/j.vacuum.2017.01.005.
[24] S. Sun, G. Singh, A. Kovacevic, C. Bruecker, Experimental and numerical investigation of tip leakage flows in a roots blower, Designs 4 (1) (2020) 3, https://doi.org/10.3390/designs4010003.
[25] G. Singh, S. Sun, A. Kovacevic, Q. Li, C. Bruecker, "Transient flow analysis in a roots blower: experimental and numerical investigations". Mechanical systems and signal processing. 2019 Dec 01; 134:106305, DOI: 10.1016/J.YMSSP.2019.106305.
[26] Q. Zhang, J. Feng, J. Wen, X. Peng, 3D transient CFD modelling of a scroll-type hydrogen pump used in FCVs, Int. J. Hydrogen. Energy 43 (41) (2018) 19231–19241, https://doi.org/10.1016/j.ijhydene.2018.08.158, 11 OctoberPages.
[27] C. Chen, Z. Wang, L. Du, D. Sun, X. Sun, Simulating unsteady flows in a compressor using immersed boundary method with turbulent wall model, Aerosp. Sci. Technol. 115 (2021) 106834, https://doi.org/10.1016/j.ast.2021.106834.
[28] Y. Tamaki, M. Harada, T. Imamura, Near-wall modification of Spalart-Allmaras turbulence model for immersed boundary method, in: 46th AIAA Fluid Dyn. Conf., 2016, pp. 1–19, https://doi.org/10.2514/1.J055824, 10.2514/6.2016-3797.
[29] S. Mojtaba Fakhari, M. Ben Hassen, H. Mr, Optimizing the operation safety and performance of an axial compressor using fluid-structure coupling and high-performance computing, Results. Eng. 18 (2023) 101061, https://doi.org/10.1016/j.rineng.2023.101061.
[30] J. Vande Voorde, J. Vierendeels, E. Dick, Flow simulations in rotary volumetric pumps and compressors with the fictitious domain method, J. Comput. Appl. Math. 168 (1–2) (2004) 491–499. Issues.
[31] J.D. Coull and N.R. Atkins, "The influence of boundary conditions on tip leakage flow," vol. 137, no. June, pp. 1–10, 2015, doi: 10.1115/1.4028796.
[32] J. Maynard, A.P.S. Wheeler, J. Taylor, R. Wells, Unsteady structure of compressor tip leakage flows, J. Turbomach. 145 (May) (2022) 1–27, https://doi.org/10.1115/1.4055769.
[33] P. Shakya, M. Thomas, AC. Seibi, M. Shekaramiz, MA.S. Masoum, Fluid-structure interaction and life prediction of small-scale damaged horizontal axis wind turbine blades, Results. Eng. 23 (2024) 102388, https://doi.org/10.1016/j.rineng.2024.102388.
[34] B. Patel; S. Rane; and A. Kovacevic, "Infrared-thermography and numerical investigation of conjugate heat transfer in roots blower", International Compressor Engineering Conference. Paper 2709. https://docs.lib.purdue.edu/icec/2709.
[35] WD. Henshaw, KK. Chand, A composite grid solver for conjugate heat transfer in fluid–structure systems, J. Comput. Phys. 228 (2009) 3708–3741, https://doi.org/10.1016/j.jcp.2009.02.007.
[36] D.-D. Dang, X.-T. Pham, P. Labbe, F. Torriano, J.-F. Morissette, C. Hudon, CFD analysis of turbulent convective heat transfer in a hydro-generator rotor-stator system, Appl. Therm. Eng. 130 (2018) 17–28, https://doi.org/10.1016/j.applthermaleng.2017.11.034.
[37] S. Rane, A. Kovačević, N. Stošić, I.K. Smith "Bi-directional system coupling for conjugate heat transfer and variable leakage gap CFD analysis of twin-screw compressors." IOP conference series. Materials Science and Engineering. 2021; 1180(1):12001, DOI: 10.1088/1757-899X/1180/1/012001.
[38] M. Matuzović, S. Rane, B. Patel, A. Kovačević, Ž. Tuković, Analysis of conjugate heat transfer in a roots blower and validation with infrared thermography, Int. J. Thermofluids. 16 (2022) 100234, https://doi.org/10.1016/j.ijft.2022.100234. Nov.
[39] H. Ding, Yu Jiang, S. Dhar, CFD modelling of coupled heat transfer between solid and fluid in a twin screw compressor, IOP Conf. Ser.: Mater. Sci. Eng. 604 (2019) 012005, https://doi.org/10.1088/1757-899X/604/1/012005.
[40] H. Ding, H. Gao, and X. Meng, "Two way coupling of CFD conjugate heat transfer simulation with solid thermal expansion in a twin screw compressor" 13th International Conference on Compressors and Their Systems, Springer Proceedings in Energy, https://doi.org/10.1007/978-3-031-42663-6_9.
[41] Z. Wang, X. Kang, S. Liu, H. Wen, H. Liu, Y. Li, A pseudo-density conjugate heat transfer method and its application to simulating the quasi-steady temperature field of a compressor cylinder, Int. Commun. Heat Mass Transf. 159 (2024) 108133, https://doi.org/10.1016/j.icheatmasstransfer.2024.108133.
[42] F. Cai, L. Zhang, H. Zhou, M. Yao and Z. Ren, "An adaptive fluid-solid coupling time step control algorithm for unsteady conjugate heat transfer", Proceedings of the Institution of Mechanical Engineers, Part C: Journal of Mechanical Engineering Science 238, Issue 16, 2024, Pages 8515–8530, https://doi.org/10.1177/09544062241238805.
[43] B. Patel, A. Kovacevic, T. Plantegenet, T. Tam, Study of leakage flow in oil-free positive displacement rotary machines using particle image velocimetry, Exp. Therm. Fluid Sci. 145 (2023) 110886, https://doi.org/10.1016/j.expthermflusci.2023.110886.
[44] M.M Doustdar, H. Kazemi, Effects of fixed and dynamic mesh methods on simulation of stepped planing craft, J. Ocean Eng. Sci. 4 (1) (2019) 33–48, https://doi.org/10.1016/j.joes.2018.12.005.
[45] J. McNaughton, I. Afgan, D.D. Apsley, S. Rolfo, T. Stallard, P.K. Stansby, A simple sliding-mesh interface procedure and its application to the CFD simulation of a tidal-stream turbine, Int. J. Numer. Methods Fluids 74 (4) (2014) 250–269, https://doi.org/10.1002/fld.3849.
[46] D. Gemayel, M. Abdelwahab, T. Ghazal, H. Aboshosha, Modelling of vertical axis wind turbine using large eddy simulations, Results. Eng. 18 (2023) 101226, https://doi.org/10.1016/j.rineng.2023.101226.
[47] Ž. Tukovic, M. Peric, H. Jasak, Consistent second-order time-accurate non-iterative PISO-algorithm, Comput. Fluids 166 (2018) 78–85, https://doi.org/10.1016/j.compfluid.2018.01.041.